Simplify your imaging workflows

Make research imaging workflows accessible, traceable, and secure with Athena Software for Core Imaging Facilities.

Thermo Scientific™ Athena Software is a premium imaging data management platform designed for core imaging facilities that support materials science research.

Athena Software ensures traceability of images, metadata, and experimental workflows through an intuitive and collaborative web interface.

Find out more at **thermofisher.com/athena**

ThermoFisher SCIENTIFIC

ADVANCED FUNCTIONAL MATERIALS
www.afm-journal.de

Highly Breathable and Stretchable Strain Sensors with Insensitive Response to Pressure and Bending

Zekun Liu, Yan Zheng, Lu Jin, Kaili Chen, Heng Zhai, Qiyao Huang, Zhongda Chen, Yangpeiqi Yi, Muhammad Umar, Lulu Xu, Gang Li, Qingwen Song, Pengfei Yue, Yi Li, and Zijian Zheng**

Wearable tensile strain sensors have aroused substantial attention on account of their exciting applications in rebuilding tactile inputs of human and intelligent robots. Conventional such devices, however, face the dilemma of both sensitive response to pressure and bending stimulations, and poor breathability for wearing comfort. In this paper, a breathable, pressure and bending insensitive strain sensor is reported, which presents fascinating properties including high sensitivity and remarkable linearity (gauge factor of 49.5 in strain 0–100%, $R^2 = 99.5\%$), wide sensing range (up to 200%), as well as superior permeability to moisture, air, and water vapor. On the other hand, it exhibits negligible response to wide-range pressure (0–100 kPa) and bending (0–75%) inputs. This work provides a new route for achieving wearing comfortable, high-performance, and anti-jamming strain sensors.

1. Introduction

Real-time tactile measurement with wearable strain sensors is an important and indispensable function in the understanding of human-machine interaction and the application for health monitoring.[1–3] Typical electrical strain sensors measure the change of electric changes of the device as a function of tensile strain through conformal contact with the surfaces of human bodies or machines. The vast majority of surface movements at the time of tensile strain also contain a combination of bending and compression, it has been very challenging to develop an anti-jamming strain sensor to detect tensile strain alone in complex conditions.[4]

Many studies in recent years attempted to improve the sensitivity (revealed by gauge factor (GF)), sensing range, and reliability of strain sensors by encapsulating conductive network configuration with elastomers (e.g. PDMS, Ecoflex).[5–7] The elastomers always lack permeability to air and sweat vapor, which brings about discomfort and even skin irritation during body sensing.[8–12] The irritation will be further enhanced with the increase of sweat vapor produced from the body in the condition of hypermetabolism. Although reported encapsulation-free fabric strain sensors exhibit a certain degree of permeability,[13,14] as a matter of fact, they also inevitably display significant responses to pressure and bending. These sensors are also far from optimum in body sensing network (BSN) to monitor health and activities, especially during diversified movements. It is highly desirable to develop a breathable, pressure and bending insensitive strain (PBIS) sensor that can freely excrete skin metabolites, and precisely measure only tensile strain on moving surfaces.

Herein, for the first time, this paper reports a highly breathable PBIS sensor, which is artistically constructed by

Z. Liu, Y. Zheng, L. Jin, H. Zhai, Z. Chen, Y. Yi, Dr. M. Umar, Dr. L. Xu, Prof. Y. Li
Department of Materials
University of Manchester
Oxford Road, Manchester M13 9PL, UK
E-mail: henry.yili@manchester.ac.uk

Z. Liu, Dr. Q. Huang, Prof. Z. Zheng
Laboratory for Advanced Interfacial Materials and Devices
Research Center for Smart Wearable Technology
Institute of Textiles and Clothing
The Hong Kong Polytechnic University
11 Yuk Choi Rd, Kowloon, Hung Hom, Hong Kong
E-mail: tczzheng@polyu.edu.hk

The ORCID identification number(s) for the author(s) of this article can be found under https://doi.org/10.1002/adfm.202007622.

DOI: 10.1002/adfm.202007622

Y. Zheng
College of Fashion Technology
Collaborative Innovation Centre of Textile and Garment Industry
Zhongyuan University of Technology
Zhengzhou 450007, China

K. Chen
Department of Materials
Imperial College London
Exhibition Road, London SW7 2AZ, UK

Prof. G. Li
National Engineering Laboratory for Modern Silk
College of Textile and Clothing Engineering
Soochow University
Suzhou 215123, China

Dr. Q. Song, Dr. P. Yue, Prof. Y. Li
School of Textile Science and Engineering
Xi'an Polytechnic University
19 Jinhua South Road, Xi'an 710048, China

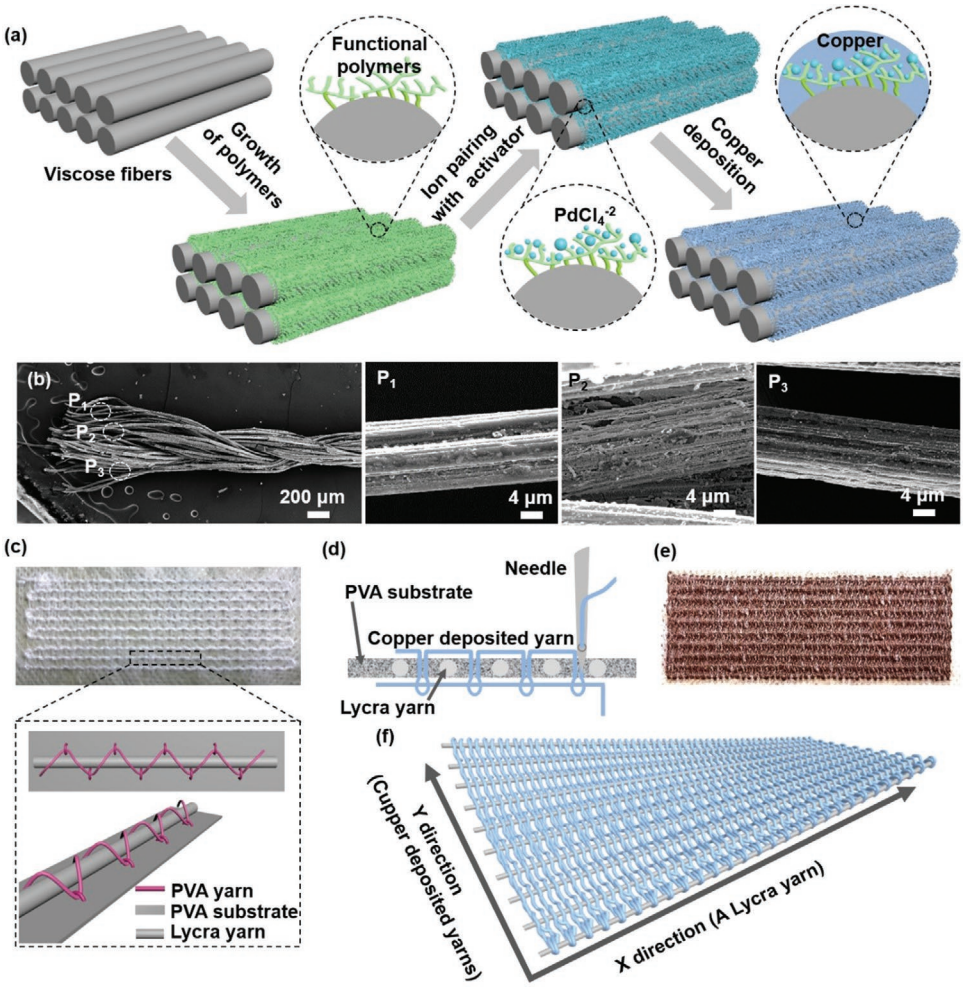

Figure 1. The schematic diagrams of conductive viscose yarn by PAMD and construction of PBIS sensor. a) The procedure of room-temperature PAMD onto viscose substrate. b) The morphology of copper deposited viscose yarn, showing the deposition can reach every single fiber. c) The image of the rectangular Lycra track (6×2.4 cm^2) fixed onto PVA substrate by PVA yarn. d) The diagram of embroidering copper deposited yarn in the Lycra track via lock-stitch embroidery. e) The surface image of the embroidery pattern with copper deposited yarn and the Lycra track. f) The diagram of the PBIS sensor after dissolving PVA, which is constructed with elastic Lycra yarn and copper deposited yarn in warp and weft direction respectively.

embroidering elastic and conductive yarns on a water-dissolvable substrate. The continuously conductive yarns make up a strain sensing network after removing the substrate. It reveals outstanding sensitivity to tensile strain, which is several orders of magnitude better than bending (GF≈ –0.09, at 75% bending) and pressure (≈0.006 kPa^{-1} at the pressure of 100 kPa). Remarkably, the sensor shows excellent linearity and high sensitivity throughout a wide sensing range (GF ≈ 49.5, 0–100% strain, and $R^2 = 0.995$). Owing to the high porosity of fabric structure, the PBIS sensor exhibits good breathability to air, moisture, and water vapor, which guarantees a wearing comfort of the microenvironment between the skin surface and the wearable sensor.

2. Results and Discussion

2.1. Fabrication Process of the PBIS Sensors

Figure 1a shows the schematic depiction of the in situ growth of copper on viscose fibers by polymer-assisted metal deposition (PAMD) reported in our previous work.[15,16] Briefly, the viscose substrate was first modified by functional polymers, that is, silane-type initiator and trimethyl ammonium chloride (METAC), following with ion pairing with palladium moieties as the activator, after which a PAMD of dense copper nanoparticles onto the viscose yarn was fulfilled from the polymer layers (see detailed procedures in Experimental Section). The pristine viscose yarn has a smooth surface (Figure S1a, Supporting Information), while a layer of serried copper nanoparticles can be observed on copper deposited viscose yarn (Figure S1b, Supporting Information). By capitalizing on PAMD, the copper deposition reaches each fiber of the twisted viscose yarn, which is verified by the fiber surface of unfasten-twist yarn (Figure 1b). The elemental composition of the viscose surface is significantly changed (Figure S1c–i, Supporting Information), where the atomic levels of C, O, and N are 58.28, 41.01, and 0.71% respectively for pristine viscose yarn. After PAMD, the content of C and O decreases by 32.89 and 10.84% respectively, while the Cu significantly increases by 56.27%. The serried copper nanoparticles on the fiber surface endow viscose yarn with low

linear resistance (≈0.23 Ω cm^{-1}). The breaking strength of the pristine yarn is ≈55 kPa, while it is more than 100 kPa after copper deposition (Figure S2, Supporting Information).

By taking advantage of pattern flexibility and high precision of embroidery technique, the PBIS sensor was exquisitely fabricated by an embroidery machine equipped with tailored fiber placement and lock-stitch embroidery (Figure S3a, Supporting Information). A pattern of rectangular nylon-covered Lycra (Figure 1c) was first stitched onto a water-soluble polyvinylalcohol (PVA) substrate by PVA yarn via tailored fiber placement (Figure S3b–d, Supporting Information). After that, two copper-deposited viscose yarns served as needle thread and bobbin thread respectively were precisely locked on the elastic yarn track (Figure 1d) by lock-stitch embroidery (Figure S3e, Supporting Information). The inter-locked pattern (Figure 1e) was then immersed in deionized water to dissolve PVA. The PBIS sensor was eventually fabricated with copper-deposited viscose yarns in the y-direction, and an elastic yarn in the x-direction (Figure 1f). Noted that the inter-locked pattern experienced a surface shrinkage (Figure S3f,g, Supporting Information) after dissolving PVA due to the pre-tension of elastic yarn during tailored fiber placement (detail in Experimental Section). The high elasticity of Lycra, and the remarkable conductivity of copper deposited viscose endow the stretchable fabric with strain sensing ability. We investigated the performance of PBIS sensors with varied densities in the

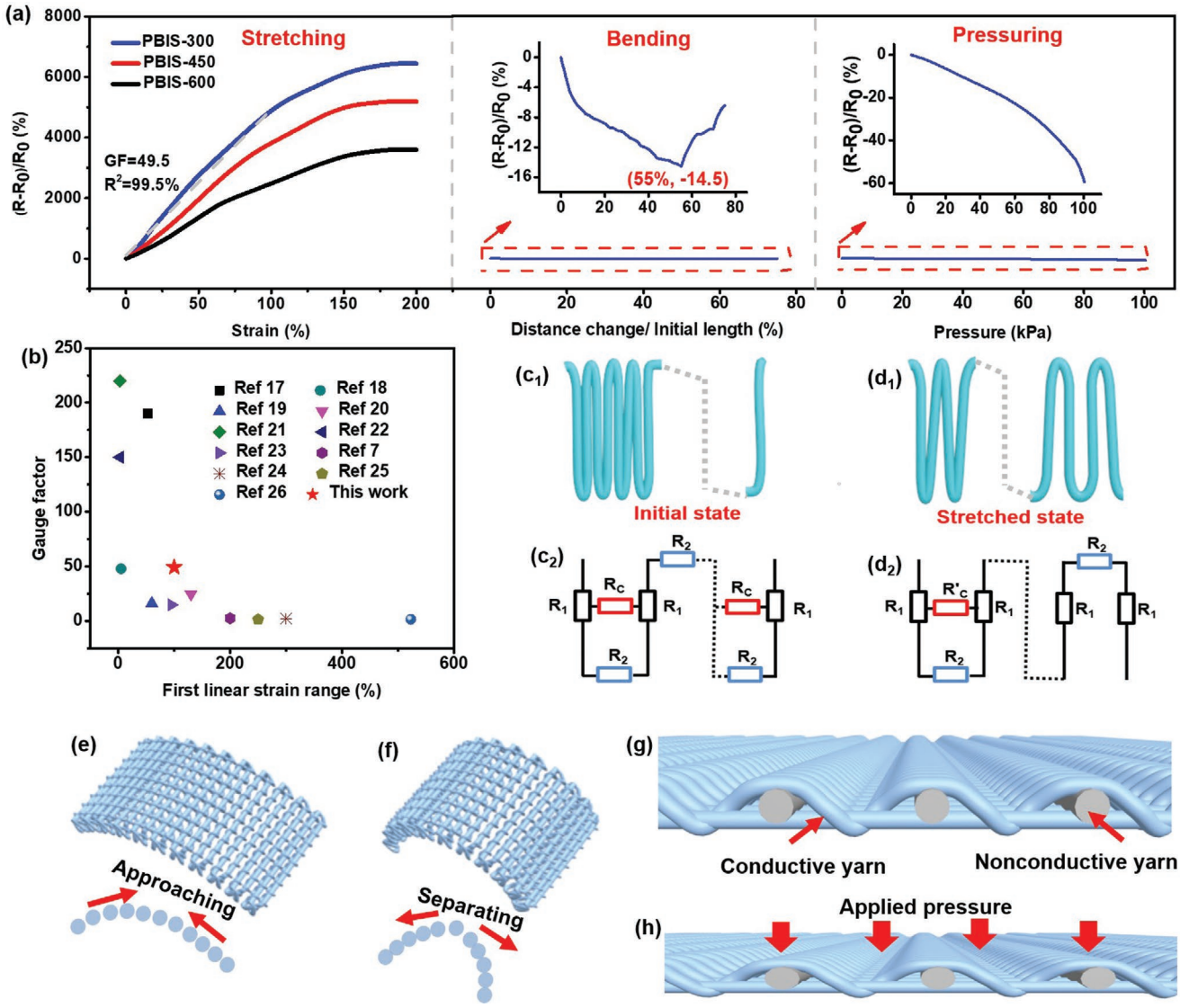

Figure 2. Electrical responses and corresponding mechanism of PBIS sensors under stretching, and bending as well as compression. a) The calibration of different-density PBIS sensors with tensile strain, and the electrical properties of PBIS-300 under bending and compression. b) Comparisons of the sensing performance in terms of first linear strain range and corresponding GF, showing the superiority of PBIS-300 than previous work. c) The initial sensing network, and corresponding resistance model. d) The stretched sensing network and corresponding resistance model. e) Schematic illustration of PBIS-300 during 0–55% bending. f) Schematic illustration of PBIS-300 during 55–75% bending. g) The sectional view of the PBIS sensor, and h) the sectional view of the PBIS sensor under applied pressure, showing the insensitivity under compression because two layers of conductive yarn are separated by non-conductive yarn.

x-direction. The sensors were denoted as PBIS-300, PBIS-450, and PBIS-600 corresponding to the devices with the distance between adjacent conductive yarns of 300, 450, and 600 μm respectively.

2.2. Calibration and Working Mechanism

The PBIS sensors show remarkable sensitivity with sufferable tensile strain up to 200%, while negligible responses to wide-range bending and pressure (**Figure 2**a). It depicts PBIS-300 acquired superior sensitivity throughout 200% tensile strain compared to PBIS-450 and PBIS-600 (linear fitting results in Table S1, Supporting Information). This could be understood that higher density PBIS possesses lower initial resistance, which corresponds to a higher relative resistance increase when tensile strain is applied. GF of all samples significantly decreases when strain reaching ≈150%, which is ascribed to the decrescent diameter of elastic yarn during the tensile process (Figure S4, Supporting Information). The smaller diameter yarn cannot prominently drive the separation of weft conductive yarns, thus the GF is slightly raised with further tensile. By contrast, the electrical response of the PBIS sensor to bending and compression is negligible. We tested the electrical properties of PBIS-300 with the inputs of wide-range bending and high pressure, it shows that the sensor acquires marginal response to both bending (GF of –0.09 at 75% bending) and high compression (0.006 kPa^{-1} at the pressure of 100 kPa). The bending was calculated by distance change/initial length of the sample during the bending test, which is shown in Figure S5, Supporting Information. The sensor has a very limited response to bending, and the resistance change to bending is almost negligible when tensile strain is over 2.5%. The resistance change of the sensor with the tensile strain of 5% is several times higher than that of the wide range of pressure input. However, it should be noted that the small tensile strain detection of most body movements by stretchable sensors seldom contains neither a high degree of bending nor very high pressure. Therefore, our sensor is always sensitive to tensile strain, insensitive to both bending and pressure in real applications. Figure S6a, Supporting Information, shows that the sensor presents a much less GF than that in the x-direction, which means the sensor enables to detect only tensile strain in x-direction. More importantly, with only a 15% y-direction strain, the force would quickly reach more than 200 N (Figure S6b, Supporting Information). The high and rapid mechanical response ensures the sensor can precisely perceive x-direction strain without disturbance, as such high force is generally unattainable in body-wearable applications. Notably, PBIS-300 presents excellent linearity (R^2 = 99.5%) with high sensitivity (GF = 49.5) from 0–100% tensile strain, which is superior to reported sensors in terms of combined GF and first linear sensing strain range (Figure 2b).[7,17–26]

The highly sensitive PBIS sensor is originated from its novel structure, of which the sensing network is constructed by conductive yarn in the x-direction. In Figure 2c, continuously conductive threads without elongation form a parallel circuit, and it becomes a hybrid circuit in the stretched state (Figure 2d). The initial resistance (R) of the sensor can be calculated with Equation (1).

$$R = n\frac{R_C R_2 + 2R_1 R_C + 2R_1 R_2}{R_C + R_2} \tag{1}$$

Where R_1, and R_2 are the resistances of the linear part and curved part of the threads respectively, and R_C refers to the contact resistance between two adjacent threads. From the initial state to a certain range of stretch, Equation (1) can depict the whole resistance of the sensor. The R increases with the increase of R_C with tensile elongation, thus leading to an incremental resistance of the sensor. With sufficient deformation, the conductive threads experience a separation. Some threads have limited contacts with surrounding threads, the contact resistance (R'_C) becomes larger. On the other hand, some threads are completely separated, and the threads form a series circuit. In this case, the resistance (R') of the sensor can be calculated with Equation (2). The above equations and models could explain the mechanism of stretch-induced increasing resistance of the sensor.

$$R' = m\frac{R'_C R_2 + 2R_1 R'_C + 2R_1 R_2}{R'_C + R_2} + (n-m)(2R_1 + R_2) \tag{2}$$

The insensitive electrical response to bending presents a diverse trend during 0–75% bending. Resistance gradually decreases when bending changes from 0–55%, which can be ascribed to the approaching of conductive threads (Figure 2e). On the contrary, an inverse increase resulted from the separation of intermediate threads (Figure 2f) arises under large-extent bending (55–75%). The marginal electrical output of the PBIS sensor to pressure benefits from the non-conductive elastic yarns between needle threads and bobbin threads. As it insulates two layers of threads (Figure 2g), the obstruct can be well maintained under applied pressure (Figure 2h).

2.3. Electromechanical Performance

Unlike conventional stretchable fabric-based strain sensors with obvious hysteresis,[13] the Lycra yarn in the PBIS sensor shows little hysteresis (Figure S7, Supporting Information). The conductive yarns are not directly subject to tensile stress nor strain during tensile elongation, while the elastic Lycra yarns can achieve good stretching ratios with very low hysteresis. This is why our PBIS sensor has shown very small hysteresis under loading-unloading cycles (**Figure 3**a). Figure 3b shows the dynamic stability by applying cyclic 10% strain with the frequency ranging from 0.1–1 Hz, and Figure 3c exhibits the dynamic strain stability from 5–180% strain with the frequency of 0.2 Hz (dynamic strain stability of PBIS-450 and PBIS-600 in Figure S8, Supporting Information). Noted that the nylon layer covered on Lycra (Figure S4, Supporting Information) is of importance to the dynamic stability of the sensor, as it can ensure the conductive threads repeatable separation and recovery during loading-uploading strain (Figure S9a–c, Supporting Information). This is confirmed by changing the covered Lycra into pure Lycra, the electrical output of the sensor made with uncovered Lycra becomes a bit unstable (Figure S9d, Supporting Information). We also demonstrate the bending and pressure responses of the sensor are stably insensitive during dynamic bending and pressure (Figure S10, Supporting Information), which guarantees the sensor can

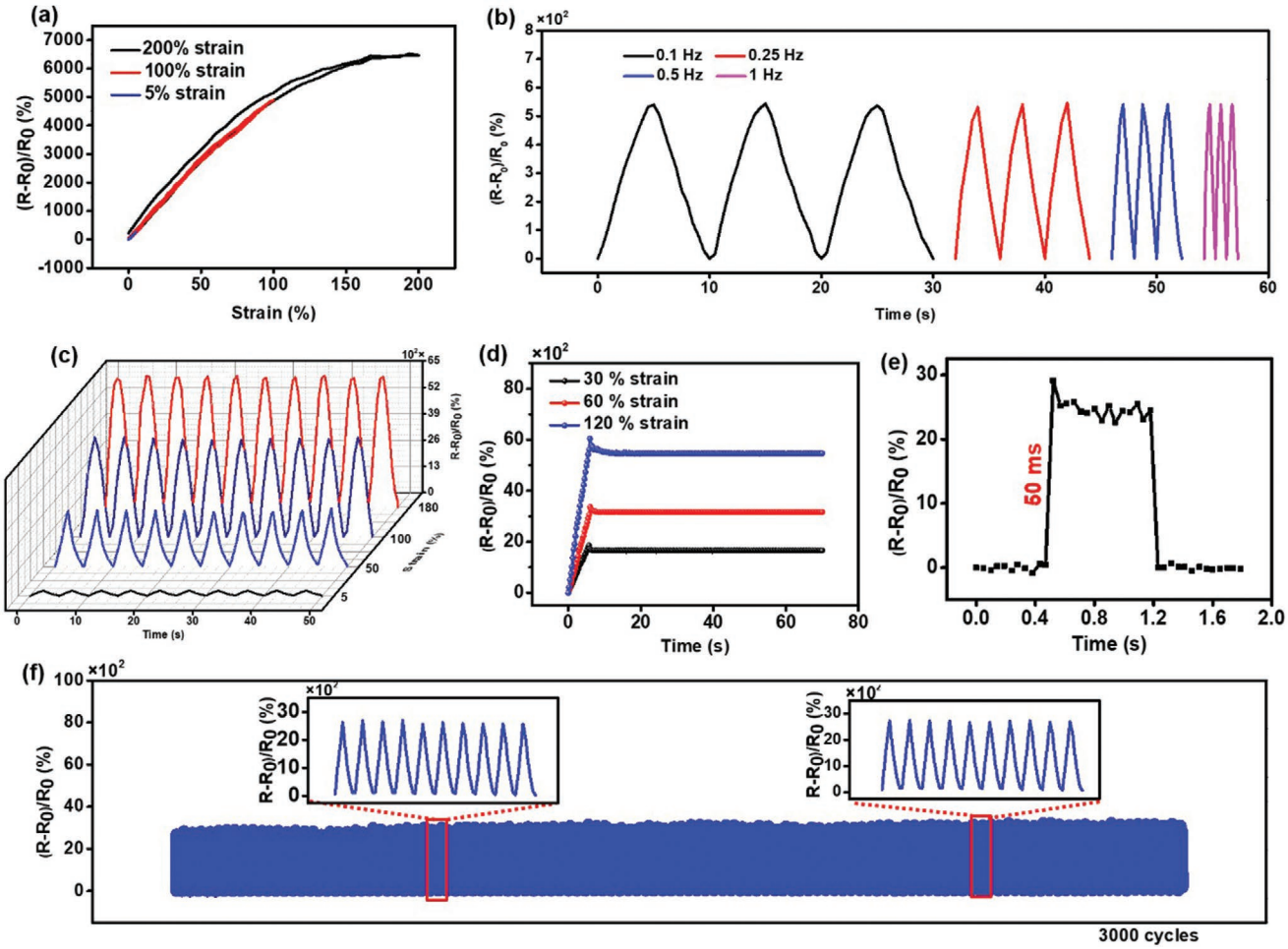

Figure 3. Electromechanical properties of PBIS-300. a) Electrical responses of different stretching–releasing strain with the speed of 20% strain S^{-1}, showing the hysteresis of the sensor. b) Dynamic stability of the sensor at various frequencies ranging from 0.1 to 1Hz. c) Dynamic stability of the sensor at various strains ranging from 5 to 180%. d) The relative resistance change of the sensor with a step strain to show low creep and static stability. e) The real-time relative resistance change of the sensor subjected to a fast-speed 0.5% strain, showing the response time can reach ≈50 ms. f) Electrical responses under 50% loading and unloading strain, with a frequency of 0.5 Hz for 3000 cycles, showing the durability of the sensor.

accurately detect tensile strain even in a complex dynamic state. By stretching the sensor by 30, 60, and 120% strain to illustrate its outstanding static stability, the electrical signal in Figure 3d shows little overshoots and swiftly remains stable.

To accurately determine its response speed, a 0.5% strain with a speed of 16 mm s^{-1} was applied to the sensor. Figure 3e displays that the responding time of the sensor reaches ≈50 ms, which can generally meet many needs of strain sensing applications. To further judge the stability and durability of the sensor, a 50% loading-uploading strain was applied to it with a frequency of 0.5 Hz for 3000 cycles. Figure 3f exhibits that the electrical response is reproducible throughout the overall fatigue with slight fluctuation, where the brilliant durability benefits from the nondestructive sensing network as well as the remarkable elasticity and robustness of Lycra (Figure S11, Supporting Information). Figure S12a, Supporting Information, presents the washing of PBIS-300 with laundry liquid at room temperature for 30 min. After washing, the calibration result in Figure S12b, Supporting Information, shows that the sensitivity of the sensor slightly decreases compared with the sensor without washing, which may be ascribed to the damage of the copper layer during the washing process. It should be noted that even with the washing process, the sensor still acquires outstanding sensitivity throughout the 200% strain, guaranteeing a good strain sensing ability. To explore the effect of wear-out issue on the electrical output of the PBIS sensor, we first tested the electrical signals of PBIS-300 by applying a recurrent 40% strain, then gave friction to the sensor by hands, and finally tested the electrical outputs again. The response of the sensor in Figure S13, Supporting Information, shows that the friction would not weaken the sensing ability and performance. From the above, the sensor shows conjunct merits of high sensitivity to tensile deformation while insensitivity to bending and pressure, remarkable linearity, outstanding stability, and durability, as well as fast responding time.

2.4. Breathability

Conventional techniques for wearable sensing always rely on components and approaches developed for strain detection outside of the real wearable environment, such sensing techniques

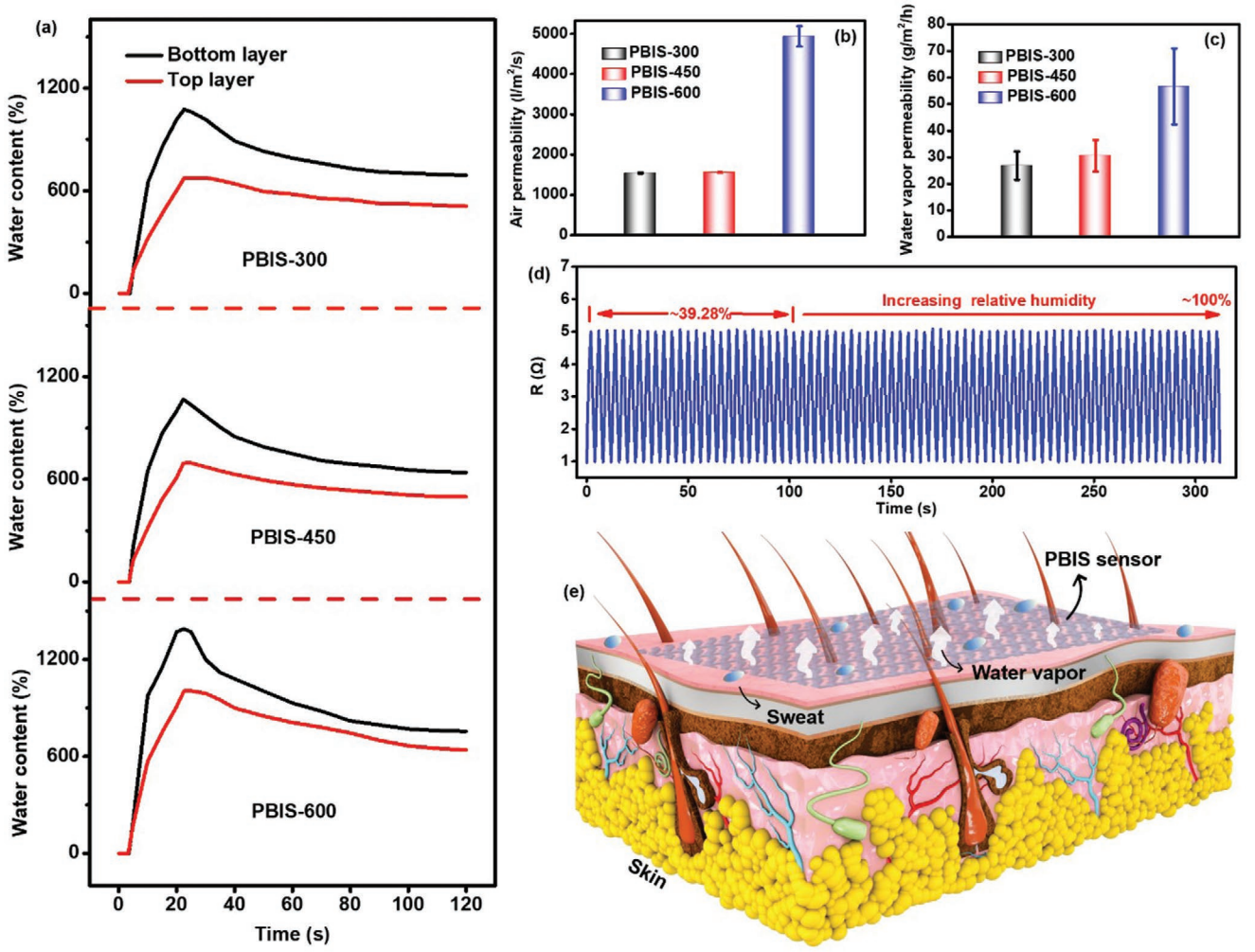

Figure 4. The breathability of PBIS sensors. a) Liquid diffusion details by applying water drops from the top layer of the sensors for 20 s, showing the remarkable moisture permeability. b) The air permeability of the sensors. c) Water vapor permeability of the sensors. d) The stable resistance change of PBIS-300 with 8% cyclic strain during ≈39.28 (room condition) to ≈100% relative humidity, showing high stability of the sensor in wide-range humidity. e) Schematic diagram of the skin-wearable sensor-environment system, as proof-of-concept illustration of PBIS sensor breathability.

may not prioritize the physical comfort of the sensing components. The encapsulation-free PBIS sensor with porous structure possesses outstanding permeability to air and vapor as well as moisture, which is of vital significance for wearing comfort. We evaluated the moisture permeability by applying several drops of water from the top layer of the sensors for 20 s, then measure the water content and track the water footprint. **Figure 4**a shows that the water drops can freely and immediately transfer from top to bottom layer (footprints in Figure S14, Supporting Information), presenting the excellent moisture permeability of all sensors. Air and vapor permeability also plays a major role in determining the wearing comfort of sensors in that human metabolites always excrete out in the forms of vapor and gas. Figure 4b,c exhibit that lower-density sample possesses better permeability to air and water vapor, as low-density sample with more pore channel for the efficient transportation of these components. It also shows that the air and water vapor permeability of all sensors exceeds 1500 l m^{-2} s^{-1} and 25 g m^{-2} h^{-1} respectively, which guarantees the sensor with outstanding breathability like general garments.

In many cases, wearable electronics implement applications in diverse environments as the humidity and temperature of air and skin surface may be totally different, especially during exercising. We tested the electrical response of PBIS-300 under recurrent 8% strain in a wide range of humidity. Figure 4d exhibits that the sensor is steady in a relative humidity of ≈39.28% (room condition), this humidity stability well maintains with an increasing relative humidity up to ≈100%. Similarly, we tested the electrical response of PBIS-300 under recurrent 10% strain (0.1 Hz) from the temperature of ≈23.2 °C (room condition) to ≈40.1 °C in a self-built device (Figure S15a, Supporting Information). Figure S15b, Supporting Information, exhibits that the electrical outputs of the sensor are not significantly affected by the temperature change, ensuring the sensor can detect body motions without the disturbance of a certain degree of temperature range. As a proof-of-concept illustration of the breathability of the PBIS sensor, we show a schematic diagram of the skin-wearable sensor-environment system in Figure 4e. It reveals the skin metabolites can freely discharge to air in the form of water vapor due to the

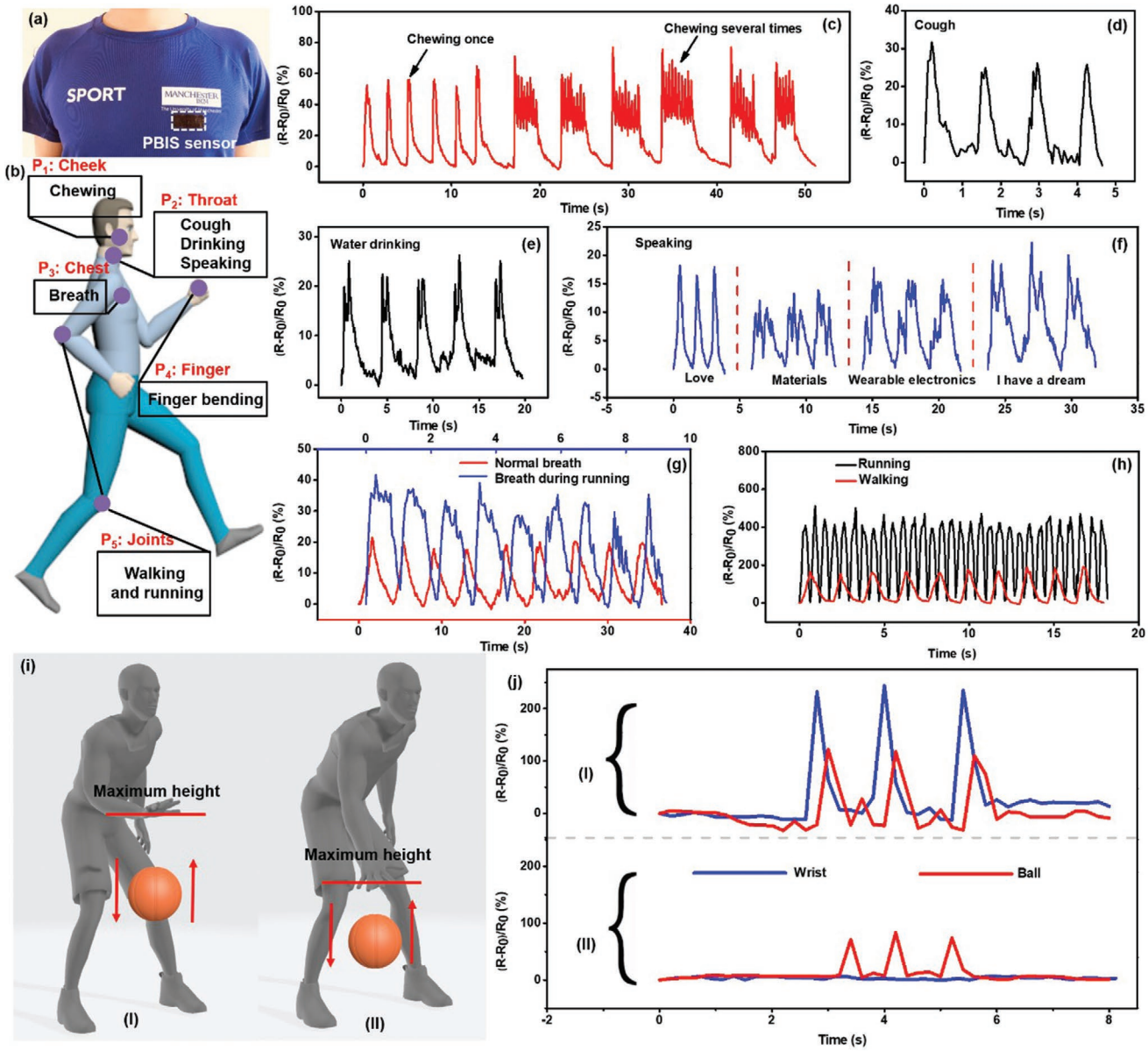

Figure 5. Applications of PBIS-300. a) Integration of the sensor with clothes, showing its good compatibility. b) An overview of the locations of BSN. c) Corresponding signals of chewing gum in different conditions by attaching the sensors to the cheek. d) Detection of the throat vibration during cough. e) Detection of human motion of drinking water. f) Signals of the throat epidermis vibration during speaking different words. g) Relative resistance changes of normal breath and breath during running. h) Detection of human walking and running styles by attaching the sensor to the knee. i) Illustration of two modes of dribbling, I) dribbling with wrist bending and the ball with a higher path, II) dribbling without wrist bending and the ball with a lower path. j) Corresponding signals of the dribbling modes collected from the sensor on the wrist and the ball.

outstanding permeability of the PBIS sensor, and the sensor can stably detect surface strain during various climate owing to the prominent humidity and temperature stability.

2.5. Applications

Different from conventional rubber-encapsulated strain sensors with poor wearability, the pure fiber-based PBIS sensor possesses good compatibility to clothes, which is essential for real wearable occasions. **Figure 5**a shows the image of a sensor-assembled cloth through the suture approach, showing the sensor can be well integrated with daily wears to implement applications. Figure 5b shows the locations of full-range BSN made with the sensor for the application of human activity recognitions spanning from tiny to large body deformations during running. Tiny body motions such as chewing, throat vibration as well as respiration can be promptly and precisely sensed by the sensor. In Figure 5c, the sensor was attached to the cheek to recognize the state of gum chewing. It displays there is an up-down resistance change for chewing once and many fluctuations for chewing several times, of which signals

are highly consistent with the expansion of masticatory muscle. For further demonstrations of detecting the tiny throat movements, we measured the relative resistance changes during cough (Figure 5d), water drinking (Figure 5e), and speaking (Figure 5f). The measurement results show that the motions are tracked with high reproducible signaling patterns for different motion activities. Figure 5g exhibits the signals of human normal breath and the breath during running, indicating a discernable respiratory rate and depth during the two diverse conditions.

In addition to tiny body movements, the broad-sensing-range sensor could also detect large body deformations. We fixed the sensor on the index finger to monitor finger bending. Electrical outputs in Figure S16a, Supporting Information, exhibit the motion is explicitly reflected by the sensor. Figure 5h shows the demonstration of monitoring motion of the knee joint during walking and running. It reveals that the movements are precisely discriminated by the response frequency and intensity of the sensor, where the walking and running speed is ≈1.8 s steps^{-1} and ≈0.59 s steps^{-1} respectively. Similarly, the diverse motions can also be well rebuilt by attaching the sensor to the arm joint (Figure S16b, Supporting Information). The sensor maintains a stable response during walking and running due to its advantage of insensitivity to pressure and bending, which has great potential applications in athletic training, sports competition as well as rehabilitation exercises (Rider monitoring in Figure S17, Supporting Information). Based on the high sensitivity, real-time recognition, broad sensing range as well as remarkable breathability, we believe the sensor can accomplish all motions rebuilding through BSN.

As a further proof-of-concept demonstration of man-machine interaction, we additionally attached the PBIS sensors to a ball and the wrist to measure the time-dependent single signal of the sensors. Figure 5i shows the two modes of dribbling, mode I represent dribbling with wrist bending and the ball with a higher path, while mode II refers to such motion without wrist bending and the ball with a lower path. In Figure 5j, by applying wrist bending for high-path dribbling, the relative resistance changes of the sensor on the wrist and the ball record the stimulations of the wrist bending and the ball swelling respectively. By contrast, low-path dribbling leads to a weaker signal from the sensor on the ball due to lower ball swelling, and the signal from the wrist sensor is stable throughout. This demonstration exhibits high application potential in dribbling correction, athletic training as well as human-computer interaction.

3. Conclusion

In summary, we have reported a brilliantly breathable, and highly sensitive strain sensor through polymer assisted copper deposition and a novel embroidery approach, which exhibits extremely low sensitivity to both pressure and bending. The all fiber-based sensors possess remarkable breathability, ennobling outstanding permeability to moisture, air as well as water vapor. The sensor with higher density (PBIS-300) shows fast response, superior environment stability, and durability, as well as high sensitivity (GF = 49.5) and prominent linearity (R^2 = 0.995) throughout the broad detection range (0–100% strain). Particularly, the creationary construction of the sensor could be rapidly extended to almost any conductive and elastic yarns, paving a new way for the low-cost and scalable fabrication of high-performance, encapsulation-free, and bending and pressure insensitive strain sensors.

4. Experimental Section

Preparation of Copper Deposited Viscose Yarn: Pristine viscose yarn (supplied by the textile fabrication lab of the University of Manchester) was first immersed into a mixed solution with 47.5 mL ethyl alcohol, 0.5 mL acetic acid, 2 mL deionized water, and 2 mL trimethoxysilane at room temperature for 2 h. After that, the silanized viscose was dipped into another aqueous mixture with 40 mL deionized water, 10 mL METAC, and 100 mg potassium persulfate at 80 °C for 1h. Then the METAC-coated viscose was immersed into 5×10^{-3} M L^{-1} $(NH_4)_2PdCl_4$ aqueous solution in room temperature and dark environment for 30 min. Finally, the $[PdCl4]^{2-}$ loaded viscose was immersed into a bath with 1:1 (v/v) mixture of solution A and B to accomplish copper deposition. Solution A is an aqueous mixture including NaOH (12g L^{-1}), $CuSO_4$ $5H_2O$ (13g L^{-1}), and $KNaC_4H_4O_6$ $4H_2O$ (29g L^{-1}) in deionized water. Solution B is a formaldehyde (9.5mL L^{-1}) aqueous solution. There is a several-time rinsing process between each procedure. The mechanism of the polymer assisted copper deposition has been reported by our previous works.[15,16]

Fabrication of PBIS Sensors: The nylon covered Lycra yarn (supplied by textile fabrication lab of University of Manchester) was first fixed by PVA yarn on a PVA substrate (from Madeira Company, Germany) via a commercial embroidery machine (JCZA 0109–550, Germany), the tension of Lycra is 0.06 N. After that, copper deposited viscose yarn was embroidered in the rectangular Lycra track (6×2.4 cm^2) by the embroidery machine. The distance between the adjacent two viscose yarns is set as 400, 600, and 800 μm to acquire different-density sensors. Finally, the sample was immersed in water to remove PVA, and the final area of the sensor is 4.5×2 cm^2. Then, the distance between viscose yarns of PBIS sensors became 300, 450, and 600 μm respectively.

Characterizations of Structure and Sensor Performance: Optical Microscope (Keyence VHX-5000) and electron microscope (electron microscope) were used to observe the morphology of pristine and copper deposited viscose yarns. The surface elements and their distribution of the yarns were obtained by the electron microscope equipped with energy-dispersive X-ray spectroscopy (EDX). Mechanical tests and electrical properties of sensors were performed using a universal testing machine (Instron 3344) and a multimeter (Keithley 2000) respectively. There were two conductive tapes as electrodes at both ends of the sensor to connect with the multimeter for signal collection. The humidity stability of the sensor was carried out in the Instron. The sensor was in a box and increasing humidity was acquired by injecting humidity into the box using a humidifier. Commercialized instruments (M021A, SDL), (M216, SDL) were used to detect the air and water vapor permeability of the sensor respectively. The moisture permeability of the sensors was reflected by testing corresponding-parameter fabrics via another commercialized instrument (M290, SDL).

Supporting Information

Supporting Information is available from the Wiley Online Library or from the author.

Acknowledgements

This work was financially supported by the EU Horizon 2020 through project ETEXWELD-H2020-MSCA-RISE-2014 (Grant No. 644268), General Research Fund of Hong Kong (PolyU 153202/16P), and the

University of Manchester through UMRI project "Graphene-Smart Textiles E-Healthcare Network" (AA14512). We also would like to thank the funding supports from Hong Kong Polytechnic University (Project 1-ZVQM) and the University Grant Council of Hong Kong (PolyU 153032/18P), as well as Key Laboratory of Silk Culture Heritage and Products Design Digital Technology, Ministry of Culture and Tourism, P. R. China.

Conflict of Interest

The authors declare no conflict of interest.

Data Availability Statement

The data that support the findings of this study are available from the corresponding authors upon request.

Keywords

breathability, copper deposition, pressure and bending insensitive, strain sensor, wearable electronics

Received: September 6, 2020
Revised: December 16, 2020
Published online: January 25, 2021

[1] S. Pan, Z. Liu, M. Wang, Y. Jiang, Y. Luo, C. Wan, D. Qi, C. Wang, X. Ge, X. Chen, *Adv. Mater.* **2019**, *31*, 1903130.
[2] T. Huang, P. He, R. Wang, S. Yang, J. Sun, X. Xie, G. Ding, *Adv. Funct. Mater.* **2019**, *29*, 1903732.
[3] C. M. Boutry, Y. Kaizawa, B. C. Schroeder, A. Chortos, A. Legrand, Z. Wang, J. Chang, P. Fox, Z. Bao, *Nat. Electron.* **2018**, *1*, 314.
[4] J. Oh, J. C. Yang, J.-O. Kim, H. Park, S. Y. Kwon, S. Lee, J. Y. Sim, H. W. Oh, J. Kim, S. Park, *ACS Nano* **2018**, *12*, 7546.
[5] Y. Gao, Q. Li, R. Wu, J. Sha, Y. Lu, F. Xuan, *Adv. Funct. Mater.* **2019**, *29*, 1806786.
[6] J. H. Lee, J. Kim, D. Liu, F. Guo, X. Shen, Q. Zheng, S. Jeon, J. K. Kim, *Adv. Funct. Mater.* **2019**, *29*, 1901623.
[7] D. Zhang, K. Zhang, Y. Wang, Y. Wang, Y. Yang, *Nano Energy* **2019**, *56*, 25.
[8] Z. Li, M. Zhu, J. Shen, Q. Qiu, J. Yu, B. Ding, *Adv. Funct. Mater.* **2019**, *30*, 1908411.
[9] W. Zeng, L. Shu, Q. Li, S. Chen, F. Wang, X. M. Tao, *Adv. Mater.* **2014**, *26*, 5310.
[10] Z. Zhao, Q. Huang, C. Yan, Y. Liu, X. Zeng, X. Wei, Y. Hu, Z. Zheng, *Nano Energy* **2020**, *70*, 104528.
[11] A. Miyamoto, S. Lee, N. F. Cooray, S. Lee, M. Mori, N. Matsuhisa, H. Jin, L. Yoda, T. Yokota, A. Itoh, *Nat. Nanotechnol.* **2017**, *12*, 907.
[12] Z. Liu, K. Chen, A. Fernando, Y. Gao, G. Li, L. Jin, H. Zhai, Y. Yi, L. Xu, Y. Zheng, H. Li, Y. Fan, Y. Li, Z. Zheng, *Chem. Eng. J.* **2021**, *403*, 126191.
[13] Z. Yang, Y. Pang, X.-l. Han, Y. Yang, J. Ling, M. Jian, Y. Zhang, Y. Yang, T.-L. Ren, *ACS Nano* **2018**, *12*, 9134.
[14] N. Karim, S. Afroj, S. Tan, P. He, A. Fernando, C. Carr, K. S. Novoselov, *ACS Nano.* **2017**, *11*, 12266.
[15] P. Li, Y. Zhang, Z. Zheng, *Adv. Mater.* **2019**, *31*, 1902987.
[16] J. Chang, J. Shang, Y. Sun, L. K. Ono, D. Wang, Z. Ma, Q. Huang, D. Chen, G. Liu, Y. Cui, Y. Qi, Z. Zheng, *Nat. Commun.* **2018**, *9*, 4480.
[17] Y. Yang, Z. Cao, P. He, L. Shi, G. Ding, R. Wang, J. Sun, *Nano Energy* **2019**, *66*, 104134.
[18] J. Zhou, X. Xu, Y. Xin, G. Lubineau, *Adv. Funct. Mater.* **2018**, *28*, 1705591.
[19] Q. Liu, J. Chen, Y. Li, G. Shi, *ACS Nano.* **2016**, *10*, 7901.
[20] K. H. Kim, N. S. Jang, S. H. Ha, J. H. Cho, J. M. Kim, *Small* **2018**, *14*, 1704232.
[21] X. Liu, C. Tang, X. Du, S. Xiong, S. Xi, Y. Liu, X. Shen, Q. Zheng, Z. Wang, Y. Wu, *Mater. Horiz.* **2017**, *4*, 477.
[22] X. Shi, S. Liu, Y. Sun, J. Liang, Y. Chen, *Adv. Funct. Mater.* **2018**, *28*, 1800850.
[23] J. Zhou, Y.-L. Hsieh, *ACS Appl. Mater. Interfaces* **2018**, *10*, 27902.
[24] Z. Qin, X. Sun, Q. Yu, H. Zhang, X. Wu, M. Yao, W. Liu, F. Yao, J. Li, *ACS Appl. Mater. Interfaces* **2020**, *12*, 4944.
[25] X. Sun, Z. Qin, L. Ye, H. Zhang, Q. Yu, X. Wu, J. Li, F. Yao, *Chem. Eng. J.* **2020**, *382*, 122832.
[26] G. Chen, H. Wang, R. Guo, M. Duan, Y. Zhang, J. Liu, *ACS Appl. Mater. Interfaces* **2020**, *12*, 6112.